SPECIFIC FEATURES OF STRUCTURE FORMATION OF SYNTHETIC HARD TOOL MATERIALS IN THE SHS COMPACTING PROCESS

E. A. Levashov, Yu. V. Bogatov, A. S. Rogachev, A. N. Pityulin, I. P. Borovinskaya, and A. G. Merzhanov

UDC 625.762.043:66.046.4

The basic specific features of structure formation and properties of a number of transient metal carbide and boride-base alloys produced by self-propagating high-temperature synthesis (SHS) of compact uniform compositions and synthetic gradient materials are considered. The main effects of the ultrasonic field on SHS compacting are emphasized. Ultrasonic oscillations are one of the effective means of controlling the structure of hard alloy materials.

STIM technology, which consists of combining the processes of combustion and pressing of hot SHS products, is one of the most promising trends in the SHS field. By this technology, it is possible to produce not only hard alloys [synthetic hard tool materials (STIM)] but also different-purpose compositions. The composition and trademark of some of them are shown in Table 1.

One of the important advantages of STIM technology is associated with the advent of a new class of alloys called SiGMa (synthetic gradient materials), possessing volume-differentiated composition and properties. While synthesizing such materials, it is possible to solve problems on designing units and parts of constructions that operate under complex conditions, e.g., under intensive wear of shock loading.

The structure formation of alloys of the STIM group consists of two main stages. At the first stage, chemical transformation of the initial reagents of a mixture into an end product occurs. After local heat initiation, a combustion wave is developed in the mixture and moves mostly with a constant velocity in the initial reagent direction. In the combustion zone on account of the reaction heat the temperature attains 2000-3000°C. The combustion zone is followed by the zones of after burning and structure formation, where the processes of nucleation, growth of crystallites, and their recrystallization reach completion.

At the second stage, the "hot" combustion products are subjected to pressing in special dies. When pressure is applied, the specimen starts intensively cooling off, thereby resulting in the final structure formation of products and in the onset of internal stresses in the material. At this stage there are three main production parameters that affect the structure and porosity of the end SHS products differently: delay time (t_d), exposure time (t_{ex}), and compacting pressure (P_c).

Thus, the structure and properties of compact SHS products are determined by a complex of physicochemical processes that proceed at the first and second SHS stages. The first stage makes a fundamental contribution to forming the microstructure of the products. Under pressing, the porosity changes to a greater degree and the grain sizes, to a lesser one.

1. "Quenching" Study of Structure Formation in SHS Wave. Since as the phase composition and the structure of a heterogeneous mixture completely change in the SHS process (the old structure breaks down and the new one is formed), of topical interest is the following problem: What processes form this or that structure of a hard alloy? "Quenching" of the SHS wave, i.e., rapid quenching or cooling of a burning sample (as a rule, of a thin charge layer) is a widespread method of studying structure formation processes. This method enables one to study the intermediate structures and SHS wave phases. The method is detailed, in particular, in [1]. The main experimental results on structure formation of hard alloys obtained by SHS wave quenching will be considered below.

Institute of Structural Macrokinetics, Russian Academy of Sciences, Chernogolovka. Translated from Inzhenerno-Fizicheskii Zhurnal, Vol. 63, No. 5, pp. 558-576, November, 1992. Original article submitted January 9, 1992.

TABLE 1

Alloy trademark	Phase composition	Initial components
STIM -1B/3	80%TiC+20%TiB_2	Ti, C, B
STIM -2	TiC+20%(Ni, Mo)	Ti, C, Ni, Mo
STIM -3B	72%TiC+18%Cr_3C_2+10%Ni	Ti, C, Cr, Ni
STIM -5	Ti(C, N)+Mo+Ni	Ti, C, Mo, Ni, TiN and other alloying components
SiGMa -1	TiC+Ni	Ti, C, Ni
SiGMa -2		

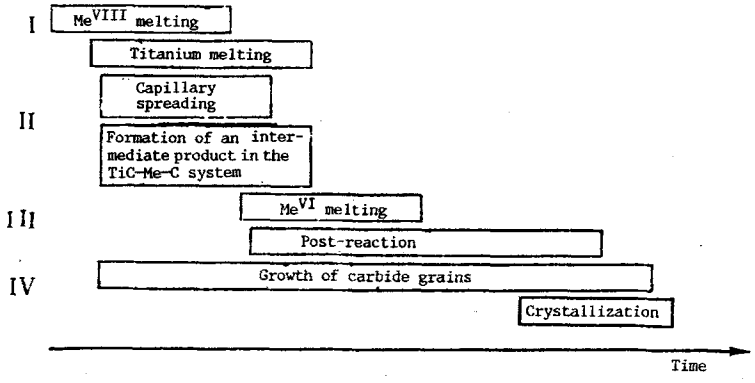

Fig. 1. Stages of forming the microstructure of SHS products in the $Ti-C-Me^{VI}-Me^{VIII}$ system.

The element composition of many materials of the STIM type is described by the $Ti-C-Me^{VI}-Me^{VIII}$ system. Here Ti and C are the basic carbide-forming elements, whose interaction releases the heat necessary for combustion, and a refractory carbide skeleton is formed, i.e., a hard alloy base; Me^{VI} is the refractory metal (or several metals) of the VI group of the Periodic Table that improves the properties of the carbide grains and the binder, as well as their adhesion to each other; Me^{VIII} is the metal (or several metals) of the iron group, based on which the hard alloy binder is formed. For example, the material of the STIM-3B type refers to the Ti–C–Cr–Ni system, and the materials of the STIM-2 type may refer to the Ti–C–Ni–Mo system or to the Ti–C–Ni subsystem. Following this terminology, the main stages of the microstructure formation may be presented schematically, as shown in Fig. 1. As is seen from this figure, many processes proceed in the combustion wave simultaneously. Therefore, the subdivision of the SHS process into four stages is rather schematic and is made mainly for convenience of the analysis.

At the first SHS stage, a metal melt containing titanium and Me^{VIII} is formed. The particles of the refractory metal (Me^{VI}) and the most coarse particles of titanium and Me^{VIII} remain unmelted. The second stage involves two processes: melt spreading over the fine-dispersed carbon material and formation of the intermediate product of the $TiC-Me^{VIII}-C$ type. Both processes start to proceed almost simultaneously. At the second stage, along with the Me^{VI} particles, the most coarse Ti and Me^{VIII} particles remain in a solid state. At the third stage the melting the metal (Me^{VI}) and of the most coarse particles of Me^{VIII} and Ti occur, thereby resulting in relatively slow post-reaction accompanied by the refractory metal saturation of the carbide grains and by the formation of the intermediate product of the type (Ti, Me^{VI}), i.e., the melt. And, finally, at the fourth stage the grains grow in the SHS product. This stage is completed with the metal melt crystallization. The last two processes, namely, the growth of grains and melt crystallization, finally arrange the microstructure and phase composition of the material.

The scheme shown in Fig. 1 is also valid for three- and two-component subsystems entering the $Ti-C-Me^{VI}$ and Me^{VIII} system, considering the evident corrections (except the items referring to Me^{VI} and Me^{VIII}).

The first two stages provide the primary structure formation and the second two, the secondary one. The primary structure formation proceeds simultaneously with the chemical transformations in the reaction zone of the SHS wave. Ti + C → TiC is the principal reaction in the system under study. Hence, the primary product must be composed of titanium carbide crystals. Experimental studies [1, 2] have shown that the primary carbide particles are 0.1-1 μm in size. This size is approximately the same when soot particles 0.1 μm in size and graphite particles 10 μm in size are used as a reagent. Thus, the size of the primary particles of the product does not directly depend on the reagent particle size. Crystallization of carbide grains may

proceed both in the melt volume and on the surface of the carbon material (if the particles of the latter are sufficiently large) when the growing carbide crystals go into the melt volume. The microprobe analysis of the quenched primary crystals in the Ti–C system has shown that their composition varies from $TiC_{0.4}$ to $TiC_{0.6}$. Adding the metal of the iron group shifts the titanium carbide compositions to the stoichiometric one. If the system contains a refractory metal (Cr, Mo, W, etc.), then its concentration in the primary titanium carbide crystals is not high, as will be seen from the results below. It is important to emphasize that for a great difference in the chemical compositions and in the dispersion degrees of the base reaction mixtures the primary products in the systems considered have much in common. As a rule, they incorporate three components: round-shaped TiC_x crystals 0.1-1 μm in size, metal melt, and hard particles of refractory or coarse-dispersed reagents that have not succeeded in reacting in the principal zone of the combustion wave. Further evolution of the microstructure is determined by interacting the above-mentioned three structure components during afterburning and subsequent cooling.

Figure 2 shows TiC–Ni alloy microstructure changes at the secondary structure formation stage. Sizes of the already formed carbide grains may increase by 1-2 orders for several seconds after the combustion front has passed. Similar changes are also observed in other alloys. In this case, the composition of the grains changes depending on what alloying metal is contained in the mixture.

In the Ti–C–Cr–Ni system the chromium concentration in the carbide grains in the afterburning zone increases gradually; even several seconds after the combustion wave has passed considerable differences in the compositions of separate carbide grains can be observed. A scatter of the compositions of separate carbide grains attains 10 mass %. Several tens of seconds are needed for the grain composition to be homogenized. In the end product, i.e., in STIM-3B/3, the carbide phase contains 71.3 ± 0.3 mass % titanium, 9.25 ± 0.3 mass % chromium, and 18.2 ± 0.2 mass % carbon according to the data of the microprobe analysis. Some part of chromium and carbon remains dissolved in the nickel-base melt. Therefore, under melt crystallization two phases are formed: metal binder and chromium-base carbide. The composition of these phases is detailed in [3].

Secondary structure formation in molybdenum-containing alloys (e.g., TiC–Mo–Ni) proceeds somewhat differently. This refractory element is not uniformly distributed in the carbide grains, forming ring structures. Depending on the charge composition and on SHS conditions the nucleus of the carbide grain contains 8 to 15 mass.% molybdenum and the grain shell, 20-40 mass %. It is also interesting to note that the nickel binder contains no more than 0.5 mass % molybdenum.

2. Specific Features of Structure Formation of Alloys under SHS Compacting. *$TiC–TiB_2$ System.* Because of the great practical interest in $TiC–TiB_2$ ceramics and the considerable efficiency of the SHS method when applied to the production of compact articles, the present work is concerned with integrated studies of structure formation processes. The $TiC–TiB_2$ system is characteristic of a simple eutectic state diagram with eutectic containing 60% TiB_2 + 40% TiC for temperatures 2520 ± 40°C [4].

During combustion of a three-component titanium–carbon–boron system two exothermal reactions forming titanium carbide and diboride proceed. In [5], an assumption has been made about the stage nature of an end product. It is based on experimental determination of the temperature and the combustion rate as a function of the initial charge component ratio. The reactions of structure formation may be subdivided in space and may proceed simultaneously in a narrow combustion zone. The latter is determined by the reactivity of the charge mixture components. Despite the assumption about the stage nature of TiC and TiB_2 formation, there are no systematic studies of the specific features of structure formation of the combustion products of the three-component Ti–C–B mixture when compact materials are obtained by SHS compacting. The powders of titanium PTM (no less than 50 μm), soot P804T, graphite ground (MPG-6) to 63-10 μm fractions, amorphous brown borium, and crystal boron were used in the present work. Three series of the mixture were prepared with different initial component ratios taken from calculation of TiC and TiB_2 formation, amounting (mass %), to: 90 + 10 (1), 80 + 20 (2), 70 + 30 (3), 60 + 40 (4), 50 + 50 (5), 40 + 60 (6), 30 + 70 (7), 20 + 80 (8), respectively. In the first series, the powders of titanium, soot, and amorphous boron were used. In the second and third series, soot and boron were replaced by their less reactive analogues. In the second series, soot was replaced by graphite and in the third series amorphous boron, by crystal boron. Synthesis was made according to the SHS compacting scheme under the conditions required to obtain the smallest porosity [6].

X-ray phase analysis has shown that irrespective of the nature and the initial component ratio only two phases – TiC and TiB_2 – are the end products. The alloy structure qualitatively changes in going from one series to another and from one ratio to another. Not only the size but also the shape of grains change. For example, in the hypoeutectic composition 1.2 (first series, ratio 80 + 20) diboride is shaped as a needle or a plate and is distributed over the boundaries of the TiC grains. Table 2 gives the mean sizes of the structural ingredients of the alloys of the $TiC–TiB_2$ system.

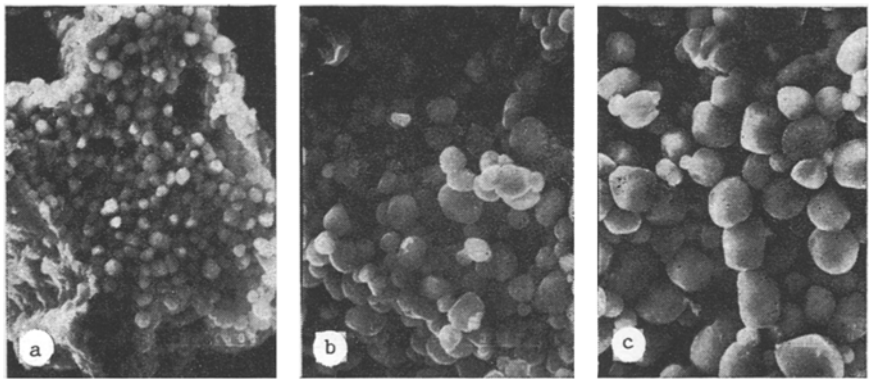

Fig. 2. Microstructures of the carbide grains of TiC–Ni alloy at the secondary structure formation stage: a) reaction zone; b) post-reaction zone; c) end product. ×2000.

TABLE 2

Composition No.	Alloy composition, mass %		Mean size of an ingredient, μm		Composition No.	Alloy composition, mass %		Mean size of an ingradient, μm	
	TiC	TiB_2	$\bar{r}_{TiC}$	$\bar{r}_{TiB_2}$		TiC	TiB_2	$\bar{r}_{TiC}$	$\bar{r}_{TiB_2}$
1.2	80	20	6	1,8	2.6	40	60	1,9	4,6
1.4	60	40	3,8	2,2	2.8	20	80	1,5	6,8
1.6	40	60	2,8	1,5	3.2	80	20	16,7	6,1
1.8	20	80	1,8	5,2	3.4	60	40	9,8	3,5
2.2	80	20	12,6	2,1	3.6	40	60	5,4	5,8
2.4	60	40	2,6	1,6	3.8	20	80	1,6	6,4

Increasing the boron content in the mixture results in substantial grinding of carbide crystals. The eutectic-composition alloy in the first series is characterized by a fine-grain uniform mixture of two phases, thus pointing to the fact that two chemical reactions proceed simultaneously and, as a result, the liquid eutectic-composition phase with a small content of the primary crystallites of TiC or TiB_2 (Fig. 3a) exists in the zone of combustion and afterburn. At a temperature below 2520°C crystallization starts followed by small formations of TiC and TiB_2. The latter do not succeed in growing because of relatively high cooling rates. In the hypoeutectic-composition alloys the product near the combustion temperature is a mixture of the liquid phase with the primary TiC crystals, and as the cooling takes place the carbide phase is formed due to a concentration segregation of eutectic on the surface of the primary crystals. The TiC grains grow, and the diboride phase is formed in the space between the grains. On the contrary, the transition to the hypereutectic region noticeably affects the size of the TiB_2 grains (see Table 2). In this case, diboride and, after the concentration segregation of eutectic, titanium carbide, are displaced by the boundaries of the TiB_2 grains.

Replacing the soot by the graphite (second series) results in a substantial change of the structure when the phase composition remains practically invariable. It is noteworthy that alloy 2.4 with the hypoeutectic ingredient ratio (Fig. 3b) has a specific eutectic structure. More coarse and strongly bonded TiC grains are observed in alloy 2.2, as compared to the similar composition of the first series (1.2). Their size attains 12.6 μm. The alloy corresponding to eutectic one (2.6) in phase composition has the microstructure similar to hypereutectic alloy 1.8: the faced crystals are located in the carbide matrix. Reducing the reactivity of carbon when soot is replaced by graphite is one of the means of widening the combustion zone. In the case of compositions 2.2-2.4 (dissolving of graphite in the titanium melt and carbide formation are the principal combustion stage), some part of the graphite continues interacting in the combustion zone up to the moment when boron is completely spent in the reaction. Thus, at any moment of time in the reaction zone of composition 2.4 the forming phase ratio TiB_2:TiC is also higher than in the combustion zone of mixtures of composition 1.4. Therefore, probably, the melt of the eutectic composition is formed which starts crystallizing before the graphite post-reaction processes are completed. This metastable state similar, in its structure, to eutectic composition 1.6 of the first series is unstable. Two-hour annealing in vacuum at T = 2100°C [7] (Fig. 3c) is sufficient to attain its equilibrium.

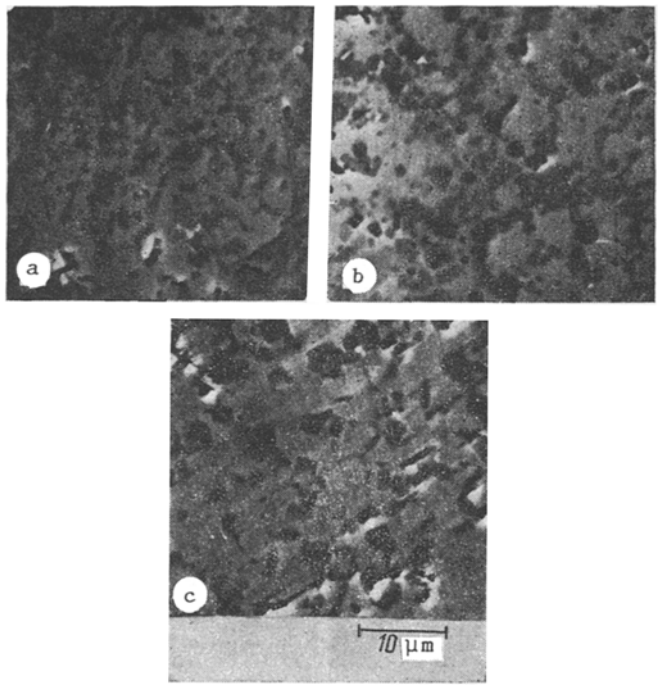

Fig. 3. SHS alloy microstructures in the TiC–TiB_2 system obtained by using soot (a) and graphite (b) at different TiC/TiB_2 ratios (mass %): 40/60 (a); 60/40 (b, c); b, 2-h annealing in vacuum at 2100°C.

We consider the structure of the alloys synthesized from the charge containing, instead of amorphous boron, its crystal analogue. In hypoeutectic alloys 3.2-3.4 both the carbide and diboride grains are coarsened. In this case, the TiB_2 phase is not uniformly distributed in the volume. The aggregates of titanium diboride in the form of parallel periodic chains that follow the contour of the combustion front surface are observed in the structure of alloy 3.2. The distance between these chains depends on the dispersion degree of the powders of titanium and crystal boron: it increases with increasing particle sizes. The discovered phenomenon may be evidently bound with the difference in the reactivity of soot and crystal boron. In the combustion zone boron does not succeed in reacting with the titanium melt, thus penetrating into the afterburning zone, where it is displaced by the carbide crystallization front into the chains, whose periodicity points to the display of auto-oscillations when the melt structure is formed. This phenomenon requires more careful study since it may find certain use in practice.

Titanium Diboride – Hardfield Steel. A three-component mixture of Ti–B–Hardfield steel 110 Mn 13 (1.10% C, 13% Mn) should be refers to systems at whose combustion and structure formation the unique potentials of the SHS process are displayed. This composite cermet arouses great interest because of the strain hardening property. This property inherent to the austenite manganese-alloyed phase (γ-iron goes into the α- and α'-phase due to deformation) enables one to use the alloy under shock loading and high-temperature wear conditions. In the present work we used powders of titanium PMT (no less than 100 μm), amorphous brown boron, and Hardfield steel 110 Mn 13 (1.10% C, 13% Mn) with a dispersion degree of no less than 100, 315, and 400-613 μm. Titanium and boron were introduced with the stoichiometric ratio to form TiB_2. Three series of mixtures with a 10, 20, 30, 40, 60% content of steel 110 Mn 13 (1.10% C, 13% Mn) were prepared. In the first series, we used the powder less than 315 μm; in the second, 400-613 μm and in the third, less than 100 μm. Mixing was made in ball 6-liter-volume mills for 10 h. Synthesis was performed according to force SHS compacting [6]. Samples were made from the synthesized sintered masses for x-ray structural (in Fe–K_α radiation) and metallographic analyses. Hardness was measured on a Vickers device. To avoid strain hardening at polishing the phase analysis was made of the surface of even spallation fragments. Also, the effect of heat treatment on the structure and properties of alloys was studied.

X-ray metallographic analysis shows that titanium diboride and iron in γ- and α-modifications are the main phase components of the combustion products. Martensite is revealed in the products made from the mixtures of the second series. On the contrary, the martensite phase is absent in SHS products of the first and second series. Introducing the powder less than

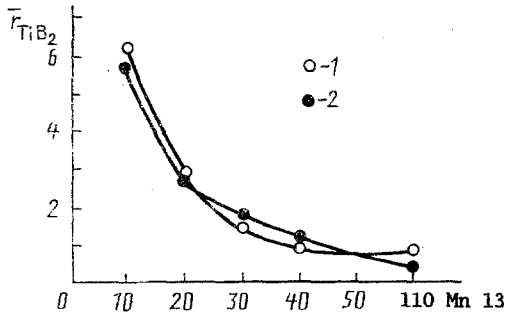

Fig. 4. Mean size of the titanium diboride grain vs Hardfield steel content in the base mixture. Dispersion degree of powder 110 Mn 13 (1.10% C, 13% Mn): 1) 400-613 μm; 2) less than 315 μm. $\bar{r}_{TiB_2}$, μm; 110 Mn 13 (1.10% C, 13% Mn), mass %.

315 μm, instead of the 400-613-μm powder, into the base exothermal mixture results in growing the γ-phase concentration. It is noteworthy that in the case of a fine-grained fraction (third series) the α-phase is not revealed by x-raying, and the products of subsequent heat treatment contain only two phases: TiB_2 and γ-iron.

The heat treatment regime greatly affects the composition of the products synthesized from the 400-613-μm powder. Elimination of the α-phase requires subsequent heat treatment of SHS products: cooling after SHS compacting up to 1100°C in a muffle furnace, 3-h exposure, and water quenching. From the metallographic data it follows that the rectangular diboride grains strongly decrease with increasing binder content in the base mixture and weakly depend on the dispersion degree of the powder 110 Mn 13 (1.10% C, 13% Mn). The mean size of the TiB_2 grain decreases from 6 to 0.5 μm with increasing the binder amount 10 to 60 mass % (Fig. 4).

When coarse particles of steel 110 Mn 13 (1.10% C, 13% Mn) are used, regions of structural and chemical inhomogeneities are observed in the products: colonies of fine TiB_2 grains, aggregates of the binder, and separate coarse TiB_2 crystals. The results on the measured hardness (HV) in the system under study agree with the x-ray phase analysis data. The alloys synthesized from the particles less than 100 μm are more plastic (less hard). At the same time the hardness of the alloys fabricated from other fractions of the steel powder may decrease only after special heat treatment.

The unusual effect of the γ-phase stabilization in the combustion wave of the three-component mixture containing powder 110 Mn 13 (1.10% C, 13% Mn) less than 100 μm in size was explained by a model experiment on remelting the 3% amorphous boron-added powder 100 Mn 13 (1.10% C, 13% Mn) in a Tamman furnace. Analysis of the specimen has shown that γ-iron is the main phase. Thus, when the alloy structure is formed in the SHS wave, some part of the boron to be introduced due to spatial separation with titanium inevitably goes into the binder and does not participate in the SHS reaction. A small titanium amount also goes into the binder. Apparently, these additions prove to be enough to obtain the pure γ-phase without requiring labor-consuming heat treatment. Also, if the separated 110 Mn 13 (1.10% C, 13% Mn) particles are not melted, or do not succeed in distributing uniformly in the volume, then the SHS products contain the boron- and titanium-depleted regions. In these regions the γ-phase may be obtained only after appropriate heat treatment involving water quenching.

The established possibility of obtaining the two-phase TiB_2–γ-iron system by the SHS method without additional heat treatment points out that SHS compacting has a high manufacturability in producing similar-type cermet compositions.

Structure Formation of a STIM-5 Alloy. High-strength tungsten-free hard alloys are being sought at present by using different production trends, including self-propagating high-temperature synthesis. To improve the properties of the titanium carbide alloy, its composition is augmented with alloy elements that increase the plasticity of the carbide phase and harden the binding phase. These elements are V, Nb, Al, W, TiN, Cr, Co, etc. [8].

Introducing niobium or niobium carbide in small amounts improves the stability of the hardening properties of an alloy [9]. This occurs because of the increasing plasticity of a carbide ingredient when niobium is dissolved in it, as well as the hardening of the binding phase.

To harden the binder the hard titanium carbide-base alloys are alloyed with aluminum [10, 11]. The latter is added in the form of a pure powder of aluminum, intermetallides in the Ni–Al system, and aluminum nitride.

Integrated alloying of the titanium carbide, nickel, and molybdenum-containing alloys with niobium, vanadium, chromium, cobalt, and other elements is aimed at improving the wear resistance at cutting with speeds up to 500 m/min [12].

Nitrogen dissolving in the carbide phase results in an additional increase of the plasticity and wear resistance of the alloy ingredient. The adverse influence of the titanium nitride (TiN) additions into hard alloys is first of all attributed to decreasing the carbide grain size [11].

Titanium nitride is usually added to alloys in the form of TiN powder or in the form of prepared carbonitride of assigned stoichiometry. Simultaneous alloying of the alloy with vanadium, aluminum, and titanium nitride hinders high-temperature deformation.

The difficulty in obtaining the assigned nitrogen content, owing to intensive denitration of the grain surface at sintering and high operating temperatures developed near the cutting edge, is a substantial drawback of the hard TiN–TiC–Ni–Mo system alloys fabricated by the traditional methods of powder metallurgy. Denitration results in the cutter stability loss.

The cutter stability may be improved by increasing the nitrogen concentration at the carbide grain center. The usual pressing–sintering scheme does not allow the nitrogen excess at the grain center to be attained.

The present work shows that the SHS compacting method can be used to fabricate multicomponent carbide- and titanium nitride-base cermet with a complex-alloyed nickel–molybdenum binder. This alloy is called STIM-5.

Metallographic studies of the alloys synthesized from the charge containing the fine-dispersed nitride-phase particles as an inert solvent enable one to assume that the nucleation and growth of the carbide phase start on the prepared TiN substrates. Heterogeneous nucleation results in forming the spherical carbonitride grains, the central part of the grains being enriched with nitrogen. The mean grain size of the wear resistance component, e.g., when plasma chemical TiN with a specific surface of 10-20 m^2/g is used, varies from 1 to 2 μm depending on the number of alloying elements. The smallest size of the Ti (CN) grains is observed at a 4% content of the titanium nitride powder in the base mixture. A characteristic double-ring structure with an outer shell from 0.3 to 0.5 μm and the inner one from 0.1 to 0.3 μm is observed in each grain. The growth of the added titanium nitride concentration above 4 mass % deteriorates the structure and properties of the alloy. This is caused by the initial conglomeration of the TiN particles and, as a consequence, by the increasing size of the titanium carbonitride particles.

At a TiN concentration less than 4%, the size of the carbonitride grains also increases. This is apparently attributed to reducing the number of titanium carbide crystallization centers. The increased tendency toward conglomeration, the difficulty in making a stable specific surface with a composition close to the granulometric one, the high cost and, accordingly, the price of the powder are the drawbacks of plasma chemical nitride powders and their manufacturing technology.

The titanium nitride powders fabricated by the technologies of a furnace synthesis and SHS lack these drawbacks despite the fact that the mean size of single TiN particles is less than 1 μm. However, after grinding in a liquid medium (alcohol, distilled water) the granulometric curve is shifted to the left practically by an order of magnitude, and the specific surface reaches 10-15 m^2/g.

The ratio of the values of the physicomechanical characteristics (hardness and strength) is mainly determined by the concentration of the main alloy ingredients such as TiN, Ni, Mo, and AlN. The most successful combinations of hardness and bending strength are 92 HRA, 115 kg/mm^2 and 91 HRA, 140 kg/mm^2. The density of the STIM-5 alloy varies, depending on the composition of the alloying elements, from 5.5 to 5.7 g/cm^3.

The unusual extremal dependence on the turning rate with a maximum of the wear resistance at cutting of structural steels is the specific feature of the STIM-5 alloy. For example, at turning of steel St3 with a depth of 2 mm, with a feed of 0.2 mm/rev the maximum of the wear resistance is observed at 150-200 m/min.

From the conclusion of the Japanese firm "Toshiba," the abrasion characteristics of tools fabricated from the STIM-5 alloy occupy an intermediate position between an tools of the type WC + Co and tools having a superhard CVD-coating.

3. Effect of the Ultrasonic Field on the Alloy Structure. In solving the problem on improving the service characteristics of hard alloy materials and articles, special attention is paid to the manufacturing techniques that allow one to effectively affect the structure and the properties of alloys. One of these techniques is the application of powerful ultrasonic oscillations [13] to an article to be sintered.

We consider the effect of the ultrasonic field on the structure and properties of compositions when the ultrasound is applied at combustion, and also at SHS compacting.

A sample pressed from a mixture of titanium carbon and nickel was put in contact with an ultrasonic transducer connected with a PMS-15A-18 converter with a working frequency of 18 kHz. The converter was energized from ultrasonic generators UZG-2-10 and UZG-3-0.4. The synthesis was made in an argon atmosphere.

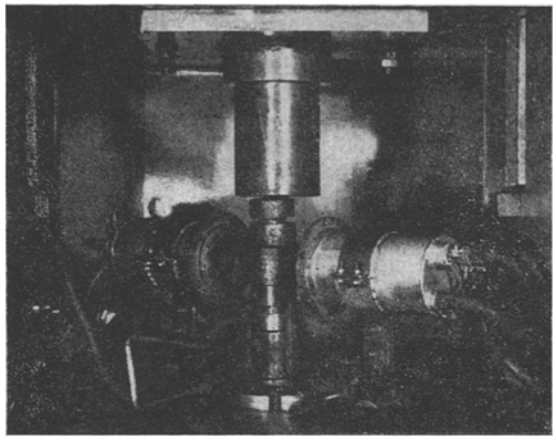

Fig. 5. Unit of the pilot plant for SHS compacting in an ultrasonic field.

Analysis of the ultrasonic field effect on combustion macrokinetics [14] permitted one to establish the following patterns. By increasing the acoustic power (the latter was determined by the travelling wave method [15]) supplied to a burning sample, the combustion rate linearly decreases 1.5-2 times. The combustion temperature in this case changes slightly. Increasing the nickel particle sizes results in increasing the ultrasonic field effect on the combustion rate. These dependences can probably be attributed to the ultrasonic capillary effect. Speeding up the spreading of an inert component over the surface of the carbon and titanium particles, the ultrasound thus reduces the value of the reaction surface in the principal zone, of the combustion wave. However, despite the increase in the afterburning zone the end products have a great conversion degree. The porosity of the end products is greatly reduced, and the microstructure is characterized by uniformly distributed carbide grains. The ultrasonic field effect signifies that all carbide particles are surrounded with the nickel sublayer.

Metallographic analysis of the SHS products has shown that by increasing the oscillation amplitude the sizes of the titanium carbide particles [14] decrease.

The established patterns point to heat and mass transfer enhancement in an ultrasonic field. The accelerated diffusion of carbon into the titanium-base melt is the cause of the growth of stoichiometry of the primary carbide crystals, and the decrease of the mean size of the titanium carbide grains is evidently bound up with reducing the surface tension forces at the growing crystal–melt interface and with homogenizing the titanium–nickel melt at the earlier stages of structure formation. Elevating the uniformity of products is attributed to the ultrasonic capillary effect. Thus, the ultrasonic field exerts a favorable influence on the structure of SHS products.

A special pilot plant (Fig. 5) representing a rigid reaction die of resonance sizes with two PMS-15A-18 converters was designed to study the effect of the ultrasonic field on the SHS compacting process. The converters connected with the UZG-2-10 generator excite the longitudinal (in the pressing direction) and bending oscillations in the die. The pressed 48-mm-diameter briquet was placed into the die, again pressed and ignited. The ultrasound was switched on simultaneously with ignition. After some delay, starting with SHS initiation sufficient for the combustion wave to travel within the entire volume of the briquet, the main pressing of the hot SHS products was made.

Studies have shown that the density and hardness of the alloys of the Ti–C–Ni and Ti–C–Cr–Ni systems increase with increasing powder (Figs. 6,7). The difference between the hydrostatic and metallographic porosities (Fig. 8) decreases in the samples exposed to sonic vibrations. This points to the uniform density distribution in the material volume. Also, considerable grinding of the carbide grains is observed. Moreover, the output of suitable qualitative specimens increases.

In the structure of the alloys containing the fourth ingredient (e.g., STIM-3B) the double carbide grain is, on the average, ground from 3.2 to 2.5 μm. In this case, a smaller content of unbonded chromium carbide Cr_3C_2 is observed in the samples fabricated under the ultrasonic field effect. Neutronographic analysis has pointed to an increase in the Cr_3C_2 concentration in double carbide.

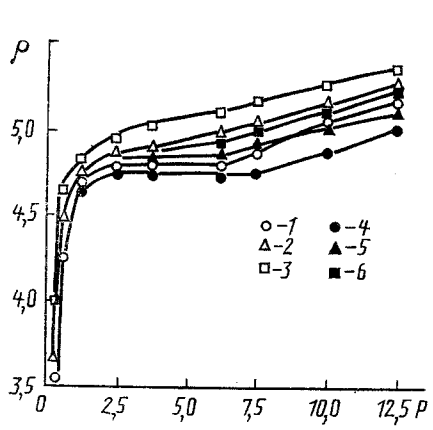

Fig. 6

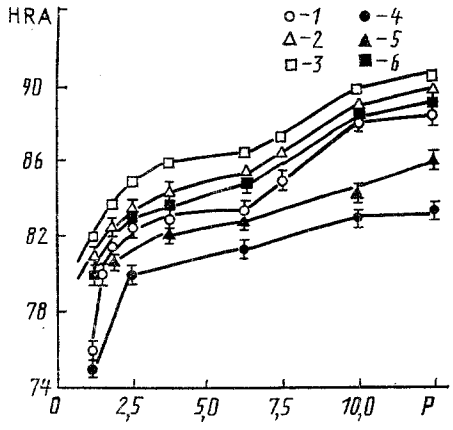

Fig. 7

Fig. 6. Density of the synthesized material TiC + 20% Ni (STIM-2) vs pressing pressure at different mixing times (h) of a charge: 17 (1, 2, 3); 5 (4, 5, 6) and ultrasonic field powers (kW): 0 (1, 4); 0.85 (2, 5); 2.3 (3, 6). ρ, g/cm^3; P, tons/cm^2.

Fig. 7. Hardness (HRA) vs pressing pressure of SHS products TiC + 20% Ni at different mixing times (h) of a charge: 17 (1, 2, 3); 5 (4, 5, 6) and at different ultrasonic field powers (kW): 0 (1,4); 0.85 (2, 5); 2.3 (3, 6).

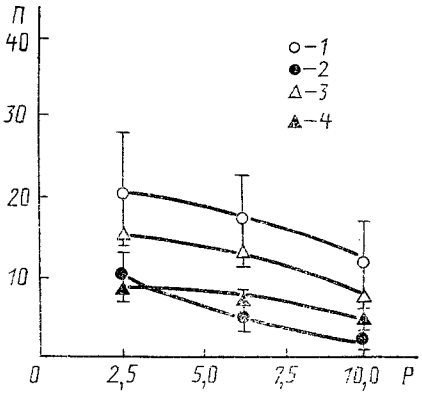

Fig. 8. Metallographic (1, 2) and hydrostatic (3, 4) porosities of the STIM-2 alloy vs pressing pressure without the ultrasonic (1, 3) and with the ultrasonic 2.3 kW (2, 4) effect. П, %.

It is interesting that the radial ultrasonic field shifts the combustion limit in the direction of the increasing values of the nickel concentration and increases the conversion degree of the carbides. So, when the ultrasonic field is absent in the Ti–C–Ni system at 60 mass % nickel, carbide $TiC_{0.78}$ is formed, and when the ultrasonic field is present, the combustion limit is shifted to 75 mass.% nickel accompanied by forming $TiC_{0.82}$. Apparently, these effects are the cause of diffusion enhancement and self-heating under interparticle friction and melt absorption of ultrasonic energy.

The favorable ultrasonic field effect on the melt structures has resulted in increasing the physicomechanical characteristics. Along with the increase of the hardness in the ultrasonic field the bending strength limit increases for the STIM-2 alloy from 1100 to 1300 MPa and for STIM-3B from 880 to 1010 MPa.

4. Effect of the Base Charge Mixture Characteristics on the Structure of the STIM Alloys. The parameters of the base exothermal mixture (charge briquet density, dispersion degree, and morphology of powders, mixing time, bulk density), the parameters that determine the temperature and SHS wave velocity (initial temperature T_0 of the process, briquet sizes, convection conditions), as well as SHS compacting regimes (pressing delay time from the moment of SHS process initiation, delay

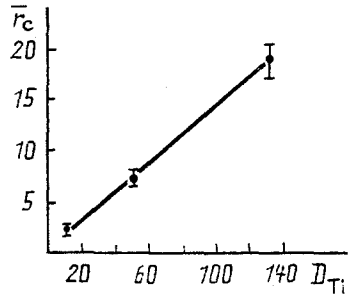

Fig. 9

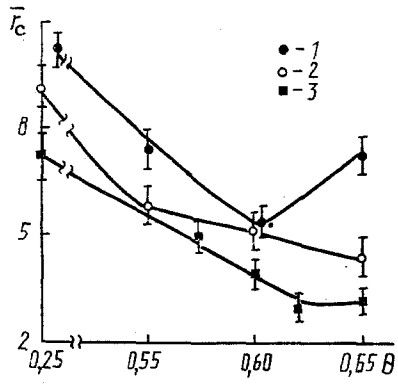

Fig. 10

Fig. 9. Dependence of the carbide particle size on the titanium powder dispersion degree in the Ti + C mixture. $\bar{r}_c$, D_{Ti}, μm.

Fig. 10. Dependence of the mean size of the carbide phase grain in the alloys fabricated by SHS compacting on the charge briquet density: 1) Ti + C; 2) Ti + C + 20% Ni; 3) STIM-3B.

time under pressing pressure, pressure of pressing or compacting) may be referred to the manufacturing techniques that allow control of the structure and properties of alloys.

We consider the effect of some of the above-mentioned controlled production and physical parameters on the structure of the end SHS products.

Study of the structure formation in the titanium–carbon system has revealed the effect of the titanium powder dispersion degree D_{Ti} on the size of the carbide crystals (Fig. 9).

Introducing, into the exothermal mixture of titanium and carbon, the powders of the binding components, whose melts wet titanium carbide (Ni, Fe, Co, Cr, Mo) or form with carbon the independent carbides (Mo_2C, Cr_3C_2, etc.), which can easily dissolve in titanium carbide, grades the above difference in the structure of SHS products when the size of the titanium powder particles varies. The size of carbide grains in the STIM-2, STIM-3B, STIM-3V, STIM-1B/3, and STIM-5 alloys varies slightly. Table 3 shows the mean size of the carbide grains as a function of the dispersion degree of the titanium powder.

The effect of the density of the reaction mixture of titanium and carbon on the combustion parameters has been studied in a number of works, e.g., [16-18]. Further study has shown that the density variation affects the mean size of titanium carbide grains in compact compositions. The above-said is supported by the dependence of the mean size of the carbide phase grain ($\bar{r}_c$) for the Ti-C, Ti-C-Ni (STIM-2), Ti–C–Cr–Ni (STIM-3B) systems shown in Fig. 10. As is seen from this figure, the quantity $\bar{r}_c$ of the STIM-3B alloys monotonically decreases with the density Θ. The dependence $\bar{r}_c(\Theta)$ is qualitatively different for a two-component system. Here, an extremum is observed at a density value equal to 0.6. As is known from [16-18], the maximum values of the combustion rate and temperature, and, hence, the conversion degree, correspond to this density. The maximum of the kinetic combustion parameters is caused by forming the largest reaction surface in the heating zone due to capillary spreading of the titanium-base melt over the carbon surface formed by the soot chains. Taking into account that the surface of each carbon particle is a potential place for a carbide phase [1] to form, an assumption may be made that the maximal number of crystallization centers of a new phase may appear at some most complete titanium wetting of the soot particles. After this, the maximum of the conversion degree in the combustion zone at a density of 0.6 results in primary crystallization of more stoichiometric titanium carbide. Bearing in mind that the mobility of the carbon atoms in stoichiometric carbide is much worse [8], the processes of crystallization and diffusion creep in the zone of structure formation of the latter proceed more slowly. This moderates the growth of the titanium carbide grains, thus determining the minimum on the curve for the dependence $\bar{r}_c = f(\Theta)$ at $\Theta = 0.6$.

The monotonic behavior of the dependences $\bar{r}_c(\Theta)$ for the STIM-2 and STIM-3B alloys may be bound with the above-mentioned fact that adding the metal of the iron group elevates the stoichiometry of the primary titanium carbide crystals. To do this, by increasing the charge briquet density the concentration of the iron group metal elevates in the fine-dispersed substructure of the melt of titanium, nickel (chromium), and carbon at an earlier stage of the structure formation (primary crystallization).

TABLE 3

Titanium dispersion degree, μm	Carbide grain size in alloy, μm			
	STIM-1B/3	STIM-2	STIM-3B	STIM-5
20—50	5—7	4—5	3—4	1—3
90—160	5—6	5—7	3—5	3—5

TABLE 4

Alloy trademark	Initial temperature, °C	Mean size of carbide grains, μm
TiC	20	5,7
	300	1,4
STIM-2	20	5,4
	300	4,3
STIM-3B	20	4,1
	300	3,8

The effect of the initial temperature on the structure of SHS products has been studied in the example of three systems. The experimental results are presented in Table 4. From this table it follows that the size of the carbide ingredient decreases for all three compositions when the initial temperature increases.

T_0 exerts the strongest influence on the graininess of the combustion products of the simple Ti–C system. Grinding the structural ingredients with increasing T_0 is apparently bound with the growth of the conversion degree in the combustion front.

We consider the effect of SHS compacting regimes on the structure of alloys. Unlike the above-considered SHS process parameters, the SHS compacting regimes do not affect substantially the grain size of the reaction products. Over a wide range (800-1750 kg/cm^2) no noticeable effect of the compacting pressure on the mean size of carbide grains and the porosity of the STIM-2, STIM-3B, and STIM-5 alloys has been revealed. However, as compared to the porous material fabricated with no pressing, the structure of a compact product can be ground 2-3 times.

The effect of the compacting pressure on the sizes of the structural ingredient is exhibited only in metals that contain no binding metal components with a lower (as compared to carbide and boride ingredients) melting point. So, for example, increasing the compacting pressure of the hot SHS products of the alloy TiC–TiB_2 (STIM-1B/3) from 870 to 1750 kg/cm^2 resulted in grinding the carbide grains 6.7-4.9 μm.

The conditions for fabricating the materials with a minimum porosity are mainly determined by the correct choice of compacting regimes such as pressing delay time and exposure time under pressure. The optimal delay time (as a rule determined empirically) must be found from the conditions of full completion of the combustion reaction, maximum possible temperature of initial pressing, and most complete removal of the initial gas powders adsorbed on the surface and soluble admixtures from the burnt specimen volume. The optimal exposure time under pressure of the burnt specimen is determined by its cooling rate and corresponds to the interval where sufficient plasticity remains. The upper bound on the time interval is set by the moment of the transition of the material from the plastic to the elastic state, and the lower bound corresponds to the time of completing the main stages of the processes of diffusional "heating" of pores and viscous flow.

Studies made recently in the field of powder metallurgy [19, 20] have shown that a further increase in the service properties of composite materials may be attained by fabricating alloys having a volume-differentiated composition and properties. A perspective in this direction is the result of a combination of the advantages of different materials in one article.

Since 1985, at the Institute of Structural Macrokinetics of the USSR Academy of Sciences, extensive studies have been made of fabricating this class of materials by the SHS process in combination with pressing. Abroad, great interest has been shown in the problem of fabricating alloys with a nonuniform distribution of ingredients by the SHS process. Most systematic studies are being made by Japanese researchers [21-25]. Such investigations have been also begun in China [26]. This class of materials is called "functionally gradient materials." As a result of the studies made at the Institute of Structural Macrokinetics, the conditions of fabricating compositions with different types of gradient of a metal-binder have been determined, the main patterns in forming their structure have been discovered, and some physicomechanical properties have been revealed.

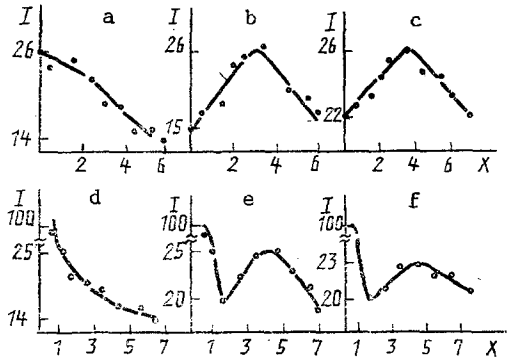

Fig. 11. Dependence of the shape of the nickel concentration profile on the compacting delay time. A nickel-to-TiC + C + 20% Ni charge layer weight ratio: a-c) 0.37; d-f) 0.64; compacting delay time. a, d) 1.0; b, e) 4.0; c, f) 10.0 sec. I, %; x, mm.

A TiC–Ni composition has been chosen as a model system. The specimen to be synthesized consists of two layers: a reaction layer of the Ti + C or Ti+ C + Ni composition, where titanium and soot have been taken in the stoichiometric ratio, and a nickel layer, which has been preliminarily pressed into 70-mm-diameter briquets. Then the specimen has been set into the die where synthesis and pressing have been carried out.

A study has been made of the effect of the compacting parameters on the shape of the nickel concentration profiles over the specimen thickness after synthesis. Figure 11 plots the variation of one of the SHS pressing parameters, namely, the delay time (t_d). (The pressing delay time is the time interval, starting with the initiation of the SHS process up to the moment when the pressure is applied.) Function I in Fig. 11 plots the sample thickness (x) variation of the relative nickel radiation intensity. The microanalysis has been made on a Superprob-733 device for two runs of experiments: at a nickel-to-reaction layer weight ratio 0.37 and 0.64 with a constant reaction layer weight of 110 g.

As is seen from this figure, two characteristic shapes of the nickel concentration profiles can be distinguished in the fabricated compositions. These are: symmetric (Fig. 11b, c) and nonsymmetric (Fig. 11a, d) or mixed (Fig. 11e, f). This shows that the structure formation may occur under qualitatively different conditions.

By using the method of thermocouple variations it has been proved, then, that forming the symmetric concentration profiles takes place under complete melting of the nickel layer to the moment when the pressing pressure is applied. In this case, in the reaction layer that contacts the nickel melt there is a space of communicating pores and, hence, impregnation is predominant at the structure formation. If, up to the pressing moment, the nickel layer does not succeed in melting, then a nonsymmetric profile develops. In this case, up to the moment of melting of the nickel layer, the space of the communicating pores is already absent in the reaction layer, and at structure formation migration [19] is predominant, which is characteristic of the nonsymmetric gradient.

In practice, cases are also encountered where the processes of impregnation and migration (Fig. 11e,f) proceed under structure formation.

Formation of nonsymmetric concentration profiles due to migration of the nickel melt into the TiC–Ni composite being in contact with the latter which has no space of communicating pores after the pressure has been applied, apparently occurs in much the same way as spontaneous migration [19] and may be described as the process of liquid flow through a dispersed structurized system where the moving force ($\Delta\Pi$) of the process is

$$\Delta\Pi = \frac{l^2\eta}{K_{per}\tau}. \qquad (1)$$

Here l is the penetration depth of the melt (in the case considered, $l \sim 10$ mm); η is the viscosity of the melt (for nickel $\eta \sim 10^{-3}$ kg/(m·sec) [27]); τ is the process time (for the compacting process it is 10 sec); K_{per} is the permeability coefficient determined according to [28] as:

$$K_{per} = \frac{1}{k}\frac{\Pi^3}{S_v^2},$$

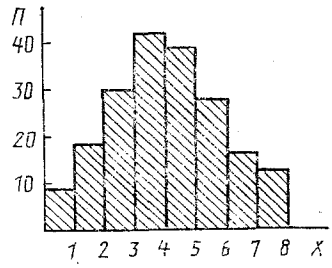

Fig. 12. Porosity distribution over the thickness of TiC_x samples.

where II is the porosity; when applied to the present case it is the volume content of the liquid phase in the TiC–N composition (0.1); S_v is the specific refractory particle surface which can be found by the formula: $S_v = 3/R$ for spherical particles with a size R; k is the coefficient dependent on the particle shape, whose value slightly differs from 1; therefore, it may be neglected.

After we have taken $R \sim 10^{-6}$ m as the size of the refractory particles, substituting all the values into expression (1) yields: $\Delta\Pi \sim 100$ MPa, which corresponds, in order of magnitude, to the value of the pressing pressure after the combustion process has ceased (a pressure of 110 MPa has been used in the experiments). This indicates that the external pressure that provides a high melt rate ($l \sim 10^{-2}$ m for $\tau \sim 10$ sec) is the moving force of the nickel melt migration process under SHS pressing.

Formation of the symmetric nickel concentration profiles cannot be caused only by the impregnation process of a porous refractory skeleton of the combustion products since it is known [19, 29] that, under the conditions of usual liquid-melt impregnation of porous bodies, concentration profiles are formed which are governed by the parabolic relationship between the impregnation depth and time ($l^2 \sim K\tau$).

From the studies it is found that in forming the symmetric concentration profiles along with the impregnation process the external pressure (~10 MPa) when applied during combustion of a reaction mixture is important. The role of the external pressure consists in forming a porous space after combustion inside the reaction layer with a symmetric porosity distribution over the thickness (Fig. 12). At the same time the value of the external pressure (~10 MPa) must not be so high that it hinders the removal of power-adsorbed gases under combustion.

After the metal-binder has been impregnated with a liquid melt, its distribution repeats the porosity distribution. Under combustion of the reaction layer, when the external pressure is absent, the porosity is uniformly distributed inside the burnt specimen. After such a skeleton has been impregnated the nickel concentration profile develops, close to the exponential distribution.

The volume gas release, which also is the cause of forming more dense surface layers and porous central ones is responsible for the asymmetric porosity gradient appearing during combustion in the two-sided pressing conditions.

Thus, it is found that the symmetric nickel concentration profile in gradient TiC–Ni compositions appears under two main conditions: the presence of the external pressure at combustion of a reaction part; melting of the nickel layer occurring before the compacting pressure is applied.

Some Physicochemical Properties of Gradient Alloys. Alloys referring to the titanium carbide–nickel system and possessing a symmetric nickel concentration profile are called SiGMa-1 (Fig. 11b), alloys with a nonsymmetric nickel concentration profile are called SiGMa-2 (Fig. 11a, d). Some physicochemical properties of the SiGMa-2 alloys have been studied. The results of the comparative tests are presented in Tables 5 and 6.

Table 5 presents the results on testing the SiGMa-1 alloy possessing a nickel concentration profile shown in Fig. 11b and uniform STIM-2 alloy (TiC–20% Ni). From this table it is seen that there are no considerable differences in the properties.

Table 6 comprises the results of the comparative tests of the SiGMa-2 alloy possessing a nickel concentration profile (Fig. 11d), a uniform STIM-3B alloy (72% TiC – 18% Cr_3C_2 – 10% Ni) and commercial hard alloys VK-20, VK-8, and T15K6. The distinctive feature of the SiGMa-2 alloy is that it is, in essence, a two-layer composite of the metal-hard alloy type where the nickel layer (2-2.5 mm) is rigidly connected with the hard alloy base (2.5-3 mm). As is seen from this table, the uniqueness of this alloy is that along with high hardness (90 HRA) it possesses high shock viscosity (up to 1.3 kg·m/cm^2) and can be recommended for fabricating from it parts and units that operate under shock loading and intensive wear conditions.

TABLE 5

Alloy trademark	Strength, kg/mm^2	Maximum and minimum hardness of a sample, HRA	Shock viscosity, kg·m/cm^2	Density, g/cm^3
SiGMa-1	80—120	85—90	0,11	5,7
STIM-2	90—120	90	0,09	5,5

TABLE 6

Alloy trademark	Shock viscosity, kg·m/cm^2	Hardness, HRA	Alloy trademark	Shock viscosity, kg·m/cm^2	Hardness, HRA
SiGMa-2	0,8—1,3	90	VK-8	0,35	87,5
STIM-3B	0,07	92,5	T15K6	0,08	90
VK-20	0,48	84	T30K4	0,07	92

Thus, these results point not only to the relationship between the parameters of the SHS process and the structure of the products to be fabricated but also to the specific means of controlling the process and, hence, to the possibility of fabricating composite materials with the assigned structure and properties.

LITERATURE CITED

1. A. G. Merzhanov, A. S. Rogachev, A. S. Mukas'yan, and B. M. Khusid, Fiz. Goreniya Vzryva, **26**, No. 1, 104-114 (1990).
2. A. S. Rogachev, V. M. Shkiro, I. D. Chausskaya, et al., Fiz. Goreniya Vzryva, **24**, No. 6, 88-92 (1988).
3. A. S. Rogachev, Yu. A. Galchenko, Z. G. Aslamazoshvili, and A. N. Pityulin, Izv. Akad, Nauk SSSR, Neorg. Mater., **22**, 1842-1844 (1986).
4. S. S. Ordan'yan, V. I. Undrod, and A. I. Avgustinik, Porosk. Metall., No. 9, 40-46 (1975).
5. V. A. Shcherbakov and A. N. Pityulin, Fiz. Goreniya Vzryva, **19**, No. 5, 24-28 (1983).
6. A. G. Merzhanov, "Self-propagating high-temperature synthesis: twenty years of searches and findings," Preprint of ISM AN SSSR, Chernogolovka (1986).
7. E. A. Levashov, I. P. Borovinskaya, Yu. V. Bogatov et al., "Specific features of the structure formation under SHS compacting of combustion products of the TiC–C–B system," Preprint of ISM AN SSSR, Chernogolovka (1990).
8. S. S. Kiparisov, Yu. V. Levinskii, and Yu. V. Petrov, Titanium Carbide. Fabrication, Properties, Application [in Russian], Moscow (1987).
9. Inventor's Certificate. USSR. MKI C22C 29/00.
10. D. Moskowitz and M. Humenik, Int. J. Powder Met., **14**, No. 1, 207-209 (1978).
11. D. Moskowitz and M. Humenik, Modern Development in Powder Metallurgy, **14**, 307-320 (1981).
12. N. Narutaki and Y. Yamane, Cut. Tool Mater. Park, 319-332 (1981).
13. B. A. Arganat, A. P. Gudovich, and L. B. Nezhevenko, Ultrasound in Power Metallurgy [in Russian], Moscow (1986).
14. V. A. Andreev, E. A. Levashov, V. M. Mal'tsev, and N. N. Khavskii, Fiz. Goreniya Vzryva, No. 6, 65-69 (1987).
15. M. N. Dubrovin, E. A. Levashov, and N. N. Khavskii, All-Union Scientific–Technical Meeting "Use of Ultrasonic Technique and Technology in Mechanical Engineering," Abstracts of Reports, Pt. 2, Moscow (1985).
16. V. M. Shkiro and I. P. Borovinskaya, Combustion Processes in Chemical Technology and Metallurgy [in Russian], Chernogolovka (1975), pp. 253-258.
17. E. A. Nekrasov, Yu. M. Maksimov, M. Kh. Ziatdinov, and A. S. Shteinberg, Fiz. Goreniya Vzryva, **14**, No. 5, 26-32 (1978).
18. A. I. Kirdyashkin, Yu. M. Maksimov, and A. G. Merzhanov, Fiz. Goreniya Vzryva, **17**, No. 16, 10-15 (1981).
19. A. F. Lisovsky, Migration of Metal Melts in Sintered Composite Bodies [in Russian], Kiev (1984).
20. E. M. Trent, Cutting of Metals [Russian translation], Moscow (1980).

21. M. Nizno, N. Yatsuanagi, J. Yeuchi, et al., Method of Producing a Multilayer Ceramic–Ceramic or Ceramic–Metal Composite Having a Gradually Changing Composition, Eur. Par. EP 255954 17.02.1988, CL COUB 35/65. Appl. Jpn. 86/187379 8.08.1986.
22. N. Sata, J. Ceram. Soc. Jpn., **97**, No. 6, 514-520 (1989).
23. H. Nakanishi, I. Tanaka, T. Okamoto, et al., J. Jpn. Soc. Powder Powder Met., **36**, No. 6, 712-715 (1986).
24. N. Yanagisawa, N. Sata, and N. Sanada, Fabrication of TiB_2–Cu Functionally Gradient Material by the SHS Process, 1st Int. Symp. FGM, Sendai (1990), pp. 179-184.
25. Y. Miyamoto, N. Nakanishi, I. Tanaka, et al., Gas Pressure Combustion Sintering of TiC-Ni, 1st Int. Symp. FGM, Sendai (1990), pp. 257-262.
26. Yi. Fu. Zhend, Run Zhang Ynan, Zheng Ling Yang, Study on the Preparation of TiB_2–Al Functionally Gradient Material by the SHS Method, 1st Int. Symp. FGM, Sendai (1990), pp. 175-178.
27. J. Smithells, Metals, Handbook [Russian translation], Moscow (1980).
28. A. V. Lykov, Heat and Mass Transfer (Handbook) [in Russian], Moscow (1972).
29. G. A. Aksel'rud and M. A. Al'tshuler, An Introduction to Capillary-Chemical Technology [in Russian], Moscow (1983).